3-4 Airborne/Spaceborne Laser Altimeter

ISHIZU Mitsuo

Topography of the global ground surface with very high vertical accuracy and fine lateral resolution enables to observe important indicators related to the global climate change such as the decay of polar ice sheets or the growth of rain forests, and to measure land activity in agriculture and at urban areas. Satellite-borne laser altimeter is expected to measure land surface with 10 cm accuracy and 100 m resolution, which is sufficient to observe these indicators or activities. Communications Research Laboratory has been studying the laser altimeter as a valuable space sensor and constructed an airborne laser altimeter for the tests of an availability flying over the sea ice off the Okhotsk coasts of Hokkaido Island. This paper reports the results of this observation as well as the recent progress of our study of a satellite-borne laser altimeter.

1 Introduction

Accelerated decay of ice-sheets in Antarctica and retreat of the Himalayan glacier have been noted as effects of global warming. A report issued by the Intergovernmental Panel on Climatic Change (ICPP) in 1995 predicted that global atmospheric temperature will rise by about two degrees by the end of the 21st century, the sea will rise by about 50 cm, and the climate will tend toward greater extremes, including remarkably high temperatures. The United Nations Environment Programme (UNEP) adopted the Framework Treaty on Climate Change at the global environmental summit in 1992 (in Rio de Janeiro) for the purpose of stabilizing the concentration of greenhouse gases in the atmosphere to effect countermeasures against global warming. The Kyoto Protocol, adopted at the third conference in 1997 by signatory nations to this treaty, has made it obligatory for advanced countries to reduce their exhausts of greenhouse gases in the five years after 2008 relative to 1990 levels (including 6% reduction for Japan, 7% reduction for the U.S., and 8%

reduction for the EU). In the sixth conference of signatory nations in July 2001, and despite the departure of the U.S., administrative guidelines for these reductions were finally adopted. The signatory states are now preparing respective domestic systems to put the Kyoto Protocol into effect as of 2002.

Along with these countermeasures it is needed to observe phenomena that serve as indices of global warming, together with observations of greenhouse gases. For this purpose, mass balance of ice sheets and height of sea level, which is relatively immune to annual climate variations, are well suited for such observations. However, the balance between snowfall and melting of ice sheets in polar regions can presently be estimated with accuracy of only 50%, since there are few sites for land-based observations. This accuracy is equivalent to a sea level variation of 0.3 cm or an ice-sheet height of 10 cm annually. Annual increases in the altitudes of Greenland and the central part of Antarctica are estimated at 2 to 5 cm, and the uncertainty mentioned above is estimated to be 1 to 2 cm annually. To measure these predicted values

at this level of accuracy over the next 5 to 10 years, it is necessary to conduct observations over a region of 10,000 km^2 or more, using an altimeter accurate up to 10 cm and perform subsequent averaging. Only a satellite-borne laser altimeter is capable of meeting these requirements[1].

A laser altimeter transmits intense pulsed laser light to the ground from an airplane or a satellite, receives the scattered light, then measures the distance to the surface based on the round-trip delay time. Simultaneous measurement of the height and attitude of the vehicle carrying the laser altimeter enables measurements of surface elevations. Since short pulsed laser light with high energy and a pulse width of about 6 ns is used, measurements with an accuracy within 10 cm can be performed only by one laser pulse. In addition, the laser spot (or "footprint") on the ground can be focused as small as 30 m in diameter when using a satellite-borne altimeter, and it thus provides very high accuracy even with sloped surfaces.

Finally, a laser with a high repetition rate enables the land topography with high density and accuracy, even at complex geographical features. The satellite-borne laser altimeter is most suitable for the observations of ice sheets and sea ice in arctic regions where observations cannot be performed from airplanes. The efficacy of satellite-borne laser altimeters in such observations has been the subject of study in various foreign countries[2][3]. Another significant advantage of the laser altimeter lies in its ability to observe the entire earth because it is capable of collecting and processing data on the satellite. The laser altimeter will thus be incorporated into exploration programs for the moon and Mars, and will be used to make comprehensive topographical maps of these celestial bodies.

Measurements by a satellite-borne laser altimeter will also permit the creation of freeboard maps of ice sheets, which will in turn allow observation of changes in ice sheets due to global warming. In observation of land areas by a laser altimeter, the influence of warming upon vegetation can be observed by surveying the vertical distribution of forests and crops, while volcanic eruptions and movements of the continental plates may also be observed by surveying crustal movements. A scanning laser altimeter can also make maps of areas in floods and landslides, thus helping to contribute to disaster-relief efforts. For this reason, laser altimeter is also expected to contribute to the progress of aerial surveys.

With respect to the past results of satellite-borne laser altimeters, NASA has taken the lead. NASA's first achievement was the Mars Observer Laser Altimeter (MOLA) installed on the Mars Observer spacecraft. However, the spacecraft collided with Mars in August 1993 as it attempted to enter into orbit around the planet. The primary goal was to observe the altitude (accuracy < 30 m) for the entire surface of Mars on a grid with a 0.2-degree mesh, and laser pulses were scheduled at 60×10^6 shots over the expected life of two years. Subsequently, the Mars Global Surveyor, launched in November 1996, was placed in orbit around Mars at an altitude of 400 km. The installed Mars Orbiter Laser Altimeter (MOLA-2) performed altitude measurement 640×10^6 times until a transmitting laser stopped responding to emission command in June 2001[4]. The laser maintained a specified output of 20 mJ/pulse until it stopped, and performed oscillations of 671×10^6 shots. The MOLA-2 had a range accuracy of 37 cm and horizontal resolution of 300 m, but the standard accuracy of altitude data was limited to about 5 m, due to the limitations on orbital accuracy. The MOLA-2 discovered a unique geoid and detailed maps of Mars, and observed clouds, snow, and such geographical features as volcanoes[5].

In terms of observations of earth, the Shuttle Laser Altimeters 1 and 2 (SLA-01, SLA-02) were launched on the Space Shuttles by NASA in 1996 and 1997[6]. These altimeters were developed using spare parts from the MOLA, modified to provide the altimeter with the ability to record laser echoes, to observe vegetation and other physical features. Sur-

Table 1	Examples of space-borne laser altimeters									
Altimeter	Mission operation	Mass	Consuming power	Laser(Nd:YAG)	Receiving telescope	Range precision	Vertical accuracy	Foot print	Spot spacing
MOLA	(2 years)	25.90kg	28.7W	40mj, 10pps	ϕ 500mm				
MOLA-2	Nov. 1996-Jun. 2001	25.85kg	34.2W	48mj, 10pps	ϕ 500mm	37.5cm	<10m	130m	330m
SLA-01	Jan. 11-20, 1996			35mj, 10pps	ϕ 380mm			100m	700m
SLA-02	Aug. 7-18, 1997								
GLAS	Late in 2002	<300kg	330W	100mj @1 μ m, 40pps	ϕ 1000mm		<1m	70m	175m
				50mj @0.5 μ m, 40pps					
VCL	1 year	126kg	220W	10mj, 242pps	ϕ 900mm	1m	1m	25m	29m
				3 lasers					

face areas between the latitudes of 28.5 degrees north and 58 degrees south were observed, due to the inclination of the orbit. In particular, the SLA-2 emitted 3×10^6 laser pulses and received 900×10^3 echoes from ocean and land. In this way the land surface elevation, sea level, cloud-top height, surface roughness, and similar features were observed. Future plans include a scheduled Geoscience Laser Altimeter System (GLAS) and a Vegetation Canopy Lidar (VCL) (to be launched on an undecided date). GLAS will be installed on the ICESAT whose inclination will be set to 94 degrees, and be launched in the second half of 2002. GLAS is to observe the mass balance of ice sheets, vertical distribution and optical density of clouds and aerosols, and survey vegetation and land topography. VCL is to observe vertical height of vegetation on the land and land topography. Table 1 lists the specifications of these laser altimeters.

To demonstrate the effectiveness of the laser altimeter, the Communications Research Laboratory has developed a laser altimeter aboard a small airplane. Observations of free-boards of drifting ice off the Okhotsk coast of Hokkaido were made using this system. Drifting ice was selected as an observation target because laser emissions toward the surface posed no safety risks to humans (i.e., no risk of eye injury while standing on the surface), and because the sea level were used as a reference plane. As a result, the measurement accuracy of the altimeter was fully demonstrated.

Observation equipments to be installed on satellites are subject to extreme restrictions on available electric power and mass, and must be resistant to vibrations and sounds during launch. The equipments must also be capable of operations without being affected by temperature variations in space. Although a laser diode (LD)-pumped solid-state laser used as a transmitter of the laser altimeter is designed for installation on a satellite, it consumes a great deal of electric power and its operating temperature range is only half of that of other electronic instruments. Accordingly, we are conducting basic research on a satellite-borne system, including research on laser design for deployment on a satellite. This report describes the development of the airborne laser altimeter, the results of observations of drifting ice, and basic research on a space-borne laser altimeter system.

Table 2	Specifications of airborne laser altimeter
Transmitting laser	LD-pumped Q-switched Nd:YAG (Laser Diode Inc.) 1064nm, 10mj, 20pps, multi-mode
Transmitting pulse	532nm, 2mj, 7ns
Transmitting telescope	Newtonian, D=72mm, 10x
Beam divergence	100μ rad
Receiving telescope	Schmidt-Cassegranian, D=203mm, f=1280mm
Receiving FOV	4mrad
Optical filter	B=1nm, transmittance 40%
Detector	Photomultiplier with micro-channel plate (Hamamatsu Photonics, R3809U) =7%, rise time 150ps
Electronics jitter	50ps$_{rms}$
Range resolution	50mm$_{rms}$ @4352m

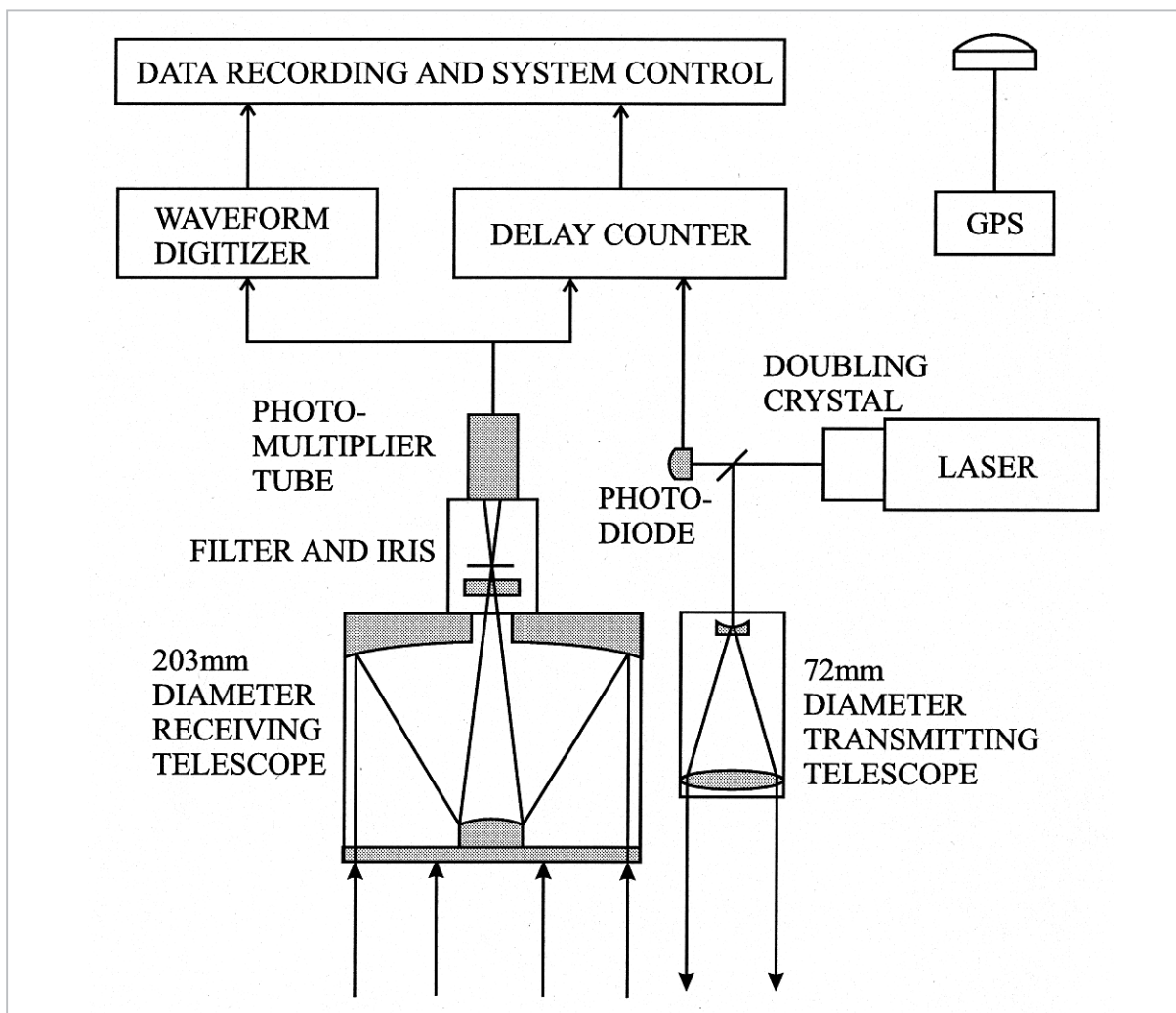## 2 Development of Airborne Laser Altimeter

The airborne laser altimeter was constructed as a system to be used in observations to test the availability of the laser altimetry. This system was basically the same as usual atmospheric lidars and consisted of a photomultiplier to detect the receiving laser echoes. The altimeter can be divided into three blocks which are a laser transmitter for generating and sending the laser light, an optical receiver for collecting scattered light on the surface and converting it into electric signals, and a data processing block to measure and record the propagation delay and waveforms of the received laser pulses. In addition, a GPS receiver is installed on the airplane to measure the altitude of the altimeter. Fig.1 shows the system block diagram; Table 2 lists the main specifications. The following sections discuss each of the block mentioned above in further detail.

2.1 Laser Transmitter/Receiver

Fig.2 shows a photograph of the laser transmitter/receiver. Fig.3 shows the view from the transmission/reception apertures. The transmitting laser at the upper right in Fig.2 is a diode-pumped Q-switched Nd:YAG laser. Since this laser is air-cooled and small in size, it is suitable for installing in an airplane, and will be free from problems of freezing coolant water even in very cold environments. The laser pulse has an output energy of 10 mJ, a pulse width of 7 ns, and a repetition frequency of 20 Hz. The pulses are sent through a KTP crystal to obtain a second harmonic of 2 mJ with a wavelength of 532 nm. The laser pulses are expanded and transmitted to the ground through a transmitting telescope
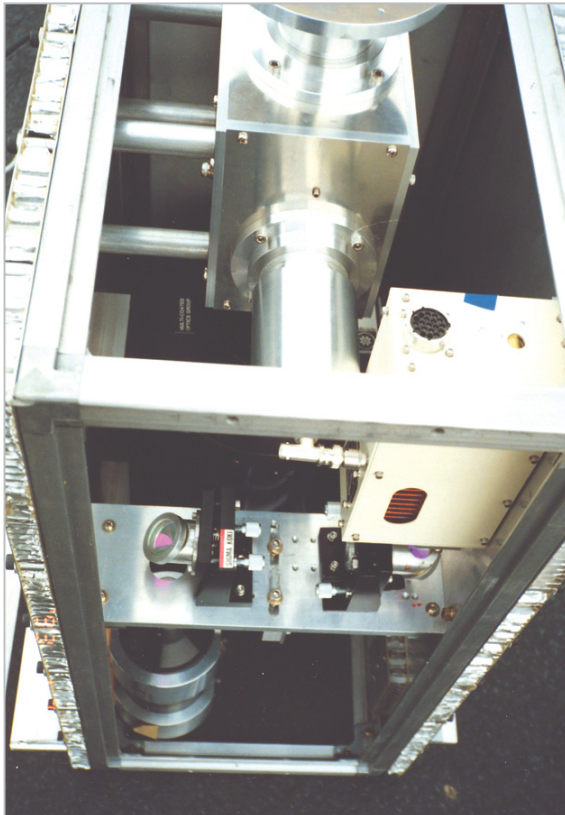
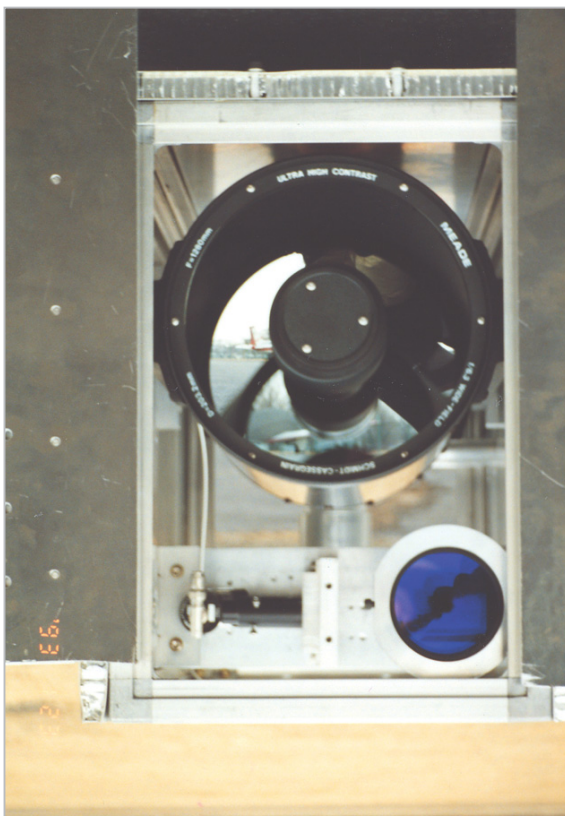**Fig.2** *Transmitter/receiver of airborne laser altimeter*

Fig.3 *Transmitter/receiver viewed from transmission/reception apertures*

(72 mm in diameter) shown at the lower left in Fig.2 to reduce the beam divergence to about 100μ rad. Assuming that the airplane is flying at an altitude of 1,000 m, the footprint of the laser pulse becomes approximately 10 cm. The transmitting time signal is obtained from the Si avalanche photodiode shown at the lower left in Fig.3 detecting the light leaked from the folding mirror which leads the laser pulse to the transmitting telescope from the laser.

The laser light scattered on the ground is collected by a Schmidt-Cassegrain telescope (203 mm in diameter) which is mounted aside the transmitting telescope (as shown in Fig.3). An interference filter, with a transmission bandwidth of 1 nm, reduces background lights from the ground. The laser echoes are then detected by the photomultiplier housed in the cylindrical aluminum case shown in the upper middle of Fig.2. To suppress background noise further, a narrower receiving field of view provides better performance. However, if this field is too narrow, optical-axis adjustments will become difficult. In this optical system, the receiving field of view is designed to cover 4 mrad, by placing an iris (5 mm in diameter) on the focal plane of the telescope. The photomultiplier is placed behind this iris, and has a rise time of 150 ps. The received signal is monitored by an oscilloscope and processed by the data processing block together with the transmitting time signal.

2.2 Data Processing Block

Since laser pulse energy changes in each pulses and also the reflectivity of the ground changes according to locations, the received pulse intensity fluctuates from pulse to pulse. Therefore, a waveform analyzer measures the precise time intervals between the leading edges of the transmitting time pulses and received pulses. Fig.4 shows the diagram of the data processing block constructed using constant fraction discriminators (CFD) as the waveform analyzer.

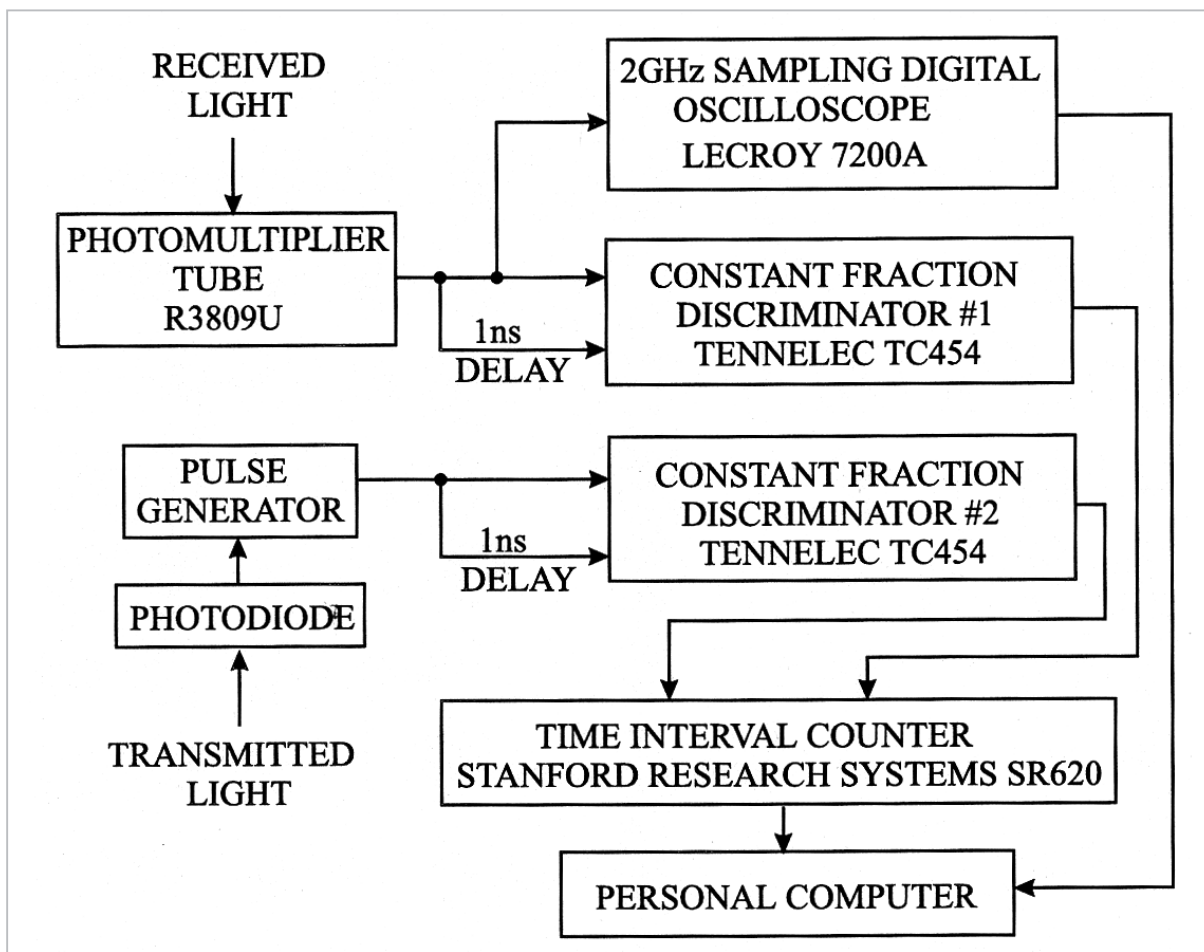The CFD detects the time at which each pulse rises to a pre-fixed level relative to each

Fig.4 *Diagram of data processing block*

peak of the pulse not affected by the magnitude or rising speed of the pulse. To prevent the CFD to detect signals by the scattered light from aerosols, ice or snow in short distances below the altimeter, the circuit is gated so as not to operate within a distance of 170 m. The time difference between the transmission and reception signals from the CFD is measured by an interval counter to obtain the propagation delay time.

The waveform of the scattered light undergoes digital conversion at a rate of 2 G sample/sec by an A/D converter installed in a commercial high-speed digital oscilloscope. If the sampling interval is 0.5 ns and the full width of the half-maximum of the laser waveform is 7 ns, the scattered laser light can be recorded in a strongly reproducible manner except for high-speed fluctuations caused by longitudinal mode-hopping in the laser pulse. This sampling period corresponds to a height

resolution of 7.5 cm. As mentioned before, the laser light is emitted with a beam divergence of 100 μ rad and the footprint will become 10 cm or less. Even when both drifting ice and sea surface are included in this spot, the laser altimeter can distinguish scattering targets of drifting ice, sea surface or ice submerged in seawater. In order to regulate the data transfer of waveform and height and to controle the electronics, the circuits are connected to a computer through GPIB.

3 Altitude Accuracy of Laser Altimeter

To enable observation by a laser altimeter aboard a satellite at lower orbit (300 to 500 km in altitude), it is necessary to ensure the eye safety of individuals on the ground. The power consumption, mass, operating temperature range, and other specifications of the

equipment must also fall within the relevant permissible ranges of the satellite. The safety standards of laser irradiation in Japan are prescribed by the Japanese Industrial Standards, which conform to standards stipulated by the International Electrotechnical Commission (IEC)[7]. According to these standards, the maximum permissible exposure (MPE) of a single laser pulse to the eyes with a pulse width of 10 ns is $MPE_{532} = 5$ mJ/m^2 at 532 nm (i.e., second harmonic of Nd:YAG laser), and $MPE_{1064} = 50$ mJ/m^2 at $= 1.064 \mu$ m, the fundamental wave.

With respect to the satellite-borne altimeter, assuming that an observer on the ground is viewing through a telescope (30 cm in diameter) and all the laser light that enter the telescope aperture passes through his pupil (7 mm in diameter), then the permissible laser intensity becomes $MPE_{532} = 2.7 \mu$ J/m^2 and $MPE_{1064} = 27 \mu$ J/m^2. Assuming that the footprint of the laser is 30 m, the allowable laser energy become 5.3 mJ and 53 mJ, respectively, which are quite small for laser altimetory from space. With an airborne altimeter in the daytime (viewable by the naked eye), the permissible laser energies are 0.04 mJ and 0.4 mJ, respectively, assuming a footprint of 10 cm. In the wavelength region of 1,400 nm to 2,600 nm (i.e., "optically safe" wavelength), however, MPE increases to between 10^3 and 10^4 J/m^2. Therefore, the transmitting energy of the satellite-borne altimeter may be permitted up to a minimum of 385 J. The laser output is not limited by the eye safety condition but by other factors as consuming electrical power, mass and cost depending on a satellite.

A technical problem for the laser altimeter in the eye-safe wavelength is that the high-speed photomultiplier with quantum-limited sensitivity operates only at a wavelength below 1 μ m. The fast photodiode that is sensitive in these regions has high quantum efficiency but no amplification capability, resulting its sensitivity being limited by dark current and amplifier noise. Such photodiodes, however, will reach to the quantum-limited sensitivity if they are used in heterodyne detections

where a local light is superposed with a signal light, and it is possible to maintain the high range accuracy[8].

The height accuracy of surface topography of the earth by the laser altimeter is synthetically determined by the range error of the laser altimeter itself, range error due to the surface slope, and accuracy of the satellite position and attitude. These errors will be described below.

For a comparison of the light detection methods the range accuracy of each altimeter system was estimated with the same transmitted energy and same diameters of the receiving telescopes. The compared detection methods consisted of (1) direct detection using a photomultiplier (PMT) for a wavelength of 532 nm, (2) direct detection using a fast photodiode (APD) for a wavelength of 1,064 nm, and (3) heterodyne detection (HET). Range accuracy was estimated for both airborne and satellite-borne altimeters. Since Q-switched pulsed lasers in the eye safe wavelength are currently under development worldwide, HET accuracy was specified for a wavelength of 1,064 nm. The diameter of the receiving telescope was set to 1 cm for the airborne altimeter, and to 15 cm for the satellite-borne altimeter. Table 4 lists the optical system parameters used in the calculation.

One significant difference between the direct detection and HET lies in the size of the transmitting/receiving field of view. The former uses discrete transmitting and receiving telescopes with different field of view, whereas the latter uses a same telescope for transmission and reception, and they have the same diffraction-limited field of view.

3.1 Range Accuracy of Altimeter
Range accuracy R is given using the S/N ratio (SNR) by

$$\Delta R = \frac{c \cdot \Delta T}{2 \cdot \sqrt{SNR}} \tag{1}$$

assuming that the laser pulse width T is 7 ns in any case, where c is the speed of light. SNR can be determined from received signal

energy Er and the noise. Er is given for distance Z by

$$Er = \frac{Et \cdot Ar \cdot To \cdot Ta^2}{Z^2} \cdot \frac{r}{\Omega} \qquad (2)$$

where Et: transmitted laser energy, Ar: receiving aperture, To: transmittance of the optical system, Ta: atmospheric transmittance, r: surface albedo, and Ω: surface scattering solid-angle. A standard ice/snow surface is assumed[9]. In this case, $\Omega = \pi$ stands for vertical incidence. For atmospheric transmittance, hazy conditions[10] (as described in the AFGL Tropospheric model) are considered. With respect to noise, background noise energy can be expressed by

$$Eb = Rt \cdot Fv \cdot Fb \cdot Ar \cdot Tg \qquad (3)$$

where Rt: intensity of scattered sunlight on the surface, Fv: receiving field of view (sr), Fb: receiving optical filter bandwidth, and Tg: receiving gate time. For the optical filter, Fb = 0.5 nm, and transmittance = 0.6, and the gate time was set as Tg = 4 ΔT. Table 3 lists the parameters for scattered sunlight on the surface and atmospheric absorption.

Table 3 Parameters of surface scattering and atmospheric absorption

Wavelength	500nm	1000nm
Surface albedo	r=0.7	r=0.5
Solar background radiation	Rt=0.025 (W/m2 srÅ)	Rt=0.016 (W/m2 srÅ)
Atmospheric transmission	Ta=0.678	Ta=0.889

By designating the number of received photons, number of background photons, detector dark current, and amplifier noise current by Nr, Nb, Id, and Ia, respectively, the SNR for respective detection systems become

$$SNR = \frac{Nr}{\sqrt{Nr + Nb + \left(\frac{Id \, \Delta T}{eG}\right)^2}} \qquad \text{(PMT)}$$

$$SNR = \frac{Nr}{\sqrt{2\left(Nr + Nb + Id\frac{Tg}{e}\right)F \, B \, Tg + \left(\frac{Ia}{e}\frac{Tg}{M}\right)^2 B}} \qquad \text{(APD)} \quad (4)$$

$$SNR = \frac{Nr}{\left(1 + \frac{Id + eNr + eNb + eIa}{Ilo}\right)B \, Tg} \qquad \text{(HET)}$$

where Nr = ηEr/hν, Nb = ηEb/hν, η: quantum efficiency of the detector, h: Planck's constant, ν: laser light frequency, Ilo: local light current for heterodyne detection, e: electric charge, G: amplification factor of PMT, M: amplification factor of APD, and F: excess noise factor. In HET, the diffraction-limitted field of view was assumed, and the optical filter bandwidth is set as equal to the amplifier bandwidth (Fb = 0.94 pm). Table 4 and 5 list the parameters of each detector and the optical system. Obtained SNR was 11, 2.8, and 900 for PMT, APD, and HET for the 1,000-m airborne altimeter, and 3.9, 0.43, and 125 for the 450-km satellite-borne altimeter, respectively. HET provides an overwhelmingly high SNR.

Table 4 Detector parameters

Specifications	PMT	Si APD	InGaP Heterodyne
Detector	R3809U (HPK*)	C30954E (EG&G)	G3476-01 (HPK*)
Gain	G=2x10⁵	M=120	1
Quantum efficiency	η=0.047	η=0.36	η=0.76
Dark current	2nA(anode)	50nA	0.8nA
Excess noise factor	-	F=4.0	-
Local power	-	-	0.5mW
Amplifier bandwidth	250MHz		
Amplifier noise	6.5pA/HZ¹ᐟ²		
Receiving aperture	10mm (airborne)/150mm (space-borne)		

Table 5 Optical-system parameters for calculation of height accuracy

detection	Airborne		Space borne	
	Direct	Heterodyne	Direct	Heterodyne
Laser energy	0.4mj		50mj	
Beam divergence (full angle)	100 μ rad	260 μ rad	100 μ rad	17 μ rad
Receiving FOV (full angle)	1mrad	260 μ rad	1mrad	17 μ rad
Transmittance of telescopes	Transmitter 0.7 Receiver 0.7			
Filter bandwidth	0.5nm	250MHz	0.5nm	250MHz
Filter transmittance	0.6	1	0.6	1

Fig.5 and 6 show the variations in range accuracy estimated from SNR as a function of flight height. In the case of direct detection with APD or PMT at low heights, the range accuracy approaches a limit determined by statistical fluctuations of the received light because the received intensity is sufficiently strong. As the height increases, the accuracy of APD tends to decrease due to the relative increase of dark current, whereas the accuracy of PMT gradually approaches the line of HET. The equivalent optical bandwidth determined by the amplifier is very narrow and the field-of-view is very small in HET detection, which leads to a lower background noise than that in the other detections. The accuracy of HET is
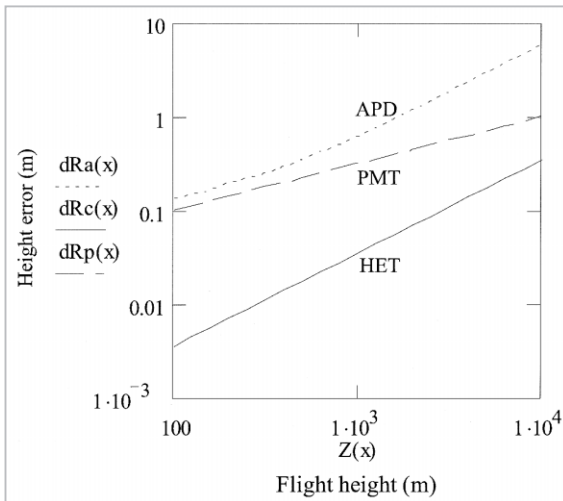
Fig.5 Range error of airborne laser altimeter

Fig.6 Range error of satellite-borne laser altimeter

ten times higher than PMT because of this low background noise as well as the high quantum efficiency of the detector. For a required accuracy of 0.1 m, neither APD nor PMT would work according to this preliminary calculation. HET could attain this accuracy for flight altitudes below 2,900 m and for orbital heights lower than 480 km. When a laser transmitts pulses in the eye-safe region, eye safety is ensured, and if the output is increased, the transmitting/receiving telescope diameter can be made even smaller. Although the receiving telescopes of the laser altimeters for earth observation shown in Table 1 have a diameter of 900 mm or more, this is extremely small as a receiving telescope and offers significant advantages in satellite deployment in terms of development schedule, manufacturing technology, and constructing cost.

3.2 Height Error Based on Surface Slope Angle

The transmitted laser beam has a beam divergence as in a radar altimeter. Consequently, height error occurs. This will be discussed for the HET laser altimeter mentioned in the previous paragraph. Let us assume that the laser altimeter located at an altitude Z (as in Fig.7) emits laser light with a beam divergence (half width) downward at an angle relative to the vertical line to the surface, with slope angle S. Because there is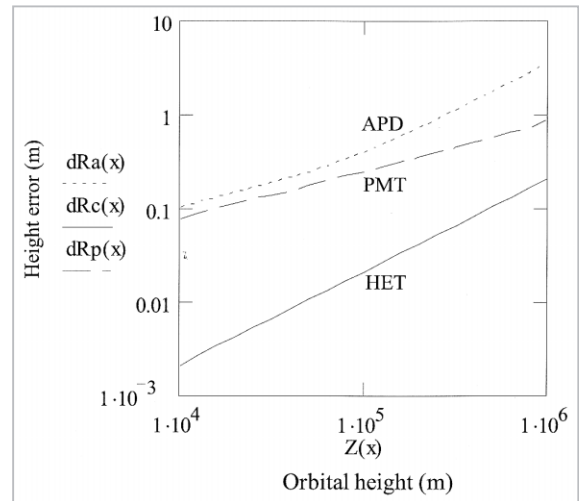 a difference between the distances to the altimeter at both ends of the diameter of the footprint, the width of the received pulse increases. This time width can be obtained by

$$\tau = \frac{2}{c} \cdot \tan(\phi + S) \cdot Z \cdot \delta \qquad (5)$$

If T in equation (1) is substituted by , the height error based on the slope angle can be found. Note that 82 % of the ice sheets in Antarctica has slope angle S = 0.01 rad (0.57 degree) or less; if a surface with this slope angle is observed by the airborne altimeter from a height of Z = 1,000 m, = 85 ps is obtained, assuming = 5 deg. From SNR = 900 in this case, the error becomes R = 0.4 mm.

In the satellite-borne altimeter, Z = 450 km and = 5 deg. are assumed. Since the transmitting/receiving telescope diameter is 15 cm, the transmitting beam divergence is as small as = 8.7 μ rad. The error becomes = 2.5 ns (R = 34 mm) from SNR = 125. This is the advantage of HET with a small footprint, whereas in the PMT system the error increases to = 29 ns (R = 2.2 m) because = 100 μ rad and SNR = 3.9.

3.3 Height Error Based on Atitude

The error included in attitude angle of the airplane expands the propagation delay time of the scattered laser light and generates the error. To find the error it is necessary to

set S = 0 and = in equation (5); the error multiplied by c/2 becomes the height error. If there is an error of = 0.01 rad (0.57 deg.) in the attitude of the airplane at a height of 1,000 m with = 5 deg. assumed, it will generate an error R = 0.87 m. To reduce this to 0.1 m, the attitude accuracy must satisfy < 1.1 mrad (0.065 deg.). When the altimeter is aboard the satellite at an altitude of 450 km, the error becomes as large as R = 390 m, and to obtain an accuracy of 0.1 m, an attitude accuracy of 2.5 μ rad is required. Therefore, it is necessary to measure the attitude with high accuracy and maintain laser emission angle at zero.

Based on the foregoing, it is determined that height error due to attitude error of the flying object is large in observations with the laser altimeter. Further, also given the height variation of the aircraft or spacecraft, it becomes important to measure its position and attitude with high accuracy. In this context, devices for measuring satellite attitude with reference to fixed stars are already in use. The use of such a device will resolve this problem.

4 Accuracy of Airborne Laser Altimeter

In observations of drifting ice with the airborne laser altimeter, the received strength becomes 5.6×10^{-12} J at a flight altitude of 1
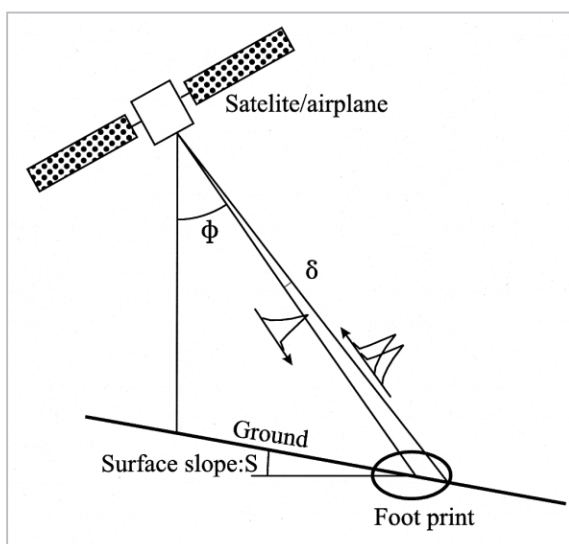

Fig.7 Height error due to surface slope angle

km based on the altimeter parameters described in Table 2, the snow and ice reflectance[11], and an optical-system transmittance of To = 0.4 (ignoring absorption by clouds and the atmosphere). Based on this strength, the number of photons obtained in the photomultiplier becomes 1.0×10^6. This value of received photons is sufficiently large, and the detector can thus operate in photocurrent mode during flight survey. The number of dark current electrons is 0.002 and may be disregarded. The background noise from the ice and snow surface is 3.5×10^{-17} j, and the number of background photoelectrons, Nb, is 6.5. The range error becomes 33 mm from equations (1) and (4), and so the height error caused by background noise is thus extremely small in the flight survey of the ice and snow surface.

For a performance test of the laser altimeter, the laser was emitted from the third floor of a building in the Communications Research Laboratory toward a television- transmitting tower 4,352 m away at night. The results indicated a distance fluctuation of 200 mm$_{pp}$ and a standard deviation of 50 mm$_{rms}$. Assuming that there was no background noise (as it was night) and that the laser light reflectivity of the iron tower was 0.5 to 0.8, the received photons becomes 7.5×10^5 to 1.2×10^6 based on the altimeter specifications. It was expected that the range error was 74 to 66 mm, based on equations (1) and (4). The standard deviation of measured values was close to the estimated range of error when reflectivity was assumed to be 0.8. Since the surface of the transmitting tower is zinc-plated, the reflectivity was considered to be consistent. From the results of this study it is concluded that the equipment performance is as expected, based on the main specifications.

5 Flight Observations

The laser altimeter was deployed in a small turbo prop airplane (CESSNA 208), which flew above the sea near Abashiri-city and above frozen Saroma Lake for observa-

tions of the ice and snow surface. Fig.8 shows a photograph of the airplane at Memanbetsu airport. It has an aperture (50 cm in diameter) for photographic topography on the inboard back deck, where the altimeter was installed. Transmission and reception of laser light to and from the surface were performed through this aperture. Moreover, a compact video cammera was attached to the altimeter to photograph the surface and permit identification of the topography and height data. The flying speed during the experiment was approximately 260 km/h, and the horizontal spacing of the laser spot on the surface was 3.6 m, based on a laser-pulse frequency of 20 Hz.

Fig.8 shows the sample observation flight path (Feb. 20, 1993). The airplane took a left turn from Abashiri harbor above the sea (sea ice 1-4), flew over the sand bank, then approached Saroma Lake (Saroma 1). Then the airplane made a round-trip over Saroma Lake, changing its direction from east to west (Saroma 2-5). Circles plotted on the path indicate the mean freeboard of the drifting ice, calculated every two seconds. Although a differential GPS base station was installed at

Fig.8 *Altimeter-bearing CESSNA 208 aircraft*

Memanbetsu airport, it failed to function, so the data from the single GPS on board the airplane was used for analysis.

Fig.10 shows the data obtained in this path, arranged chronologically in two rows. The upper plotted points of each row represent the distribution of height data from the altimeter (left vertical axis). The line plotted on the lower edge of the distribution represents the distance from the airplane to the sea surface, estimated based on the height data (left vertical axis).

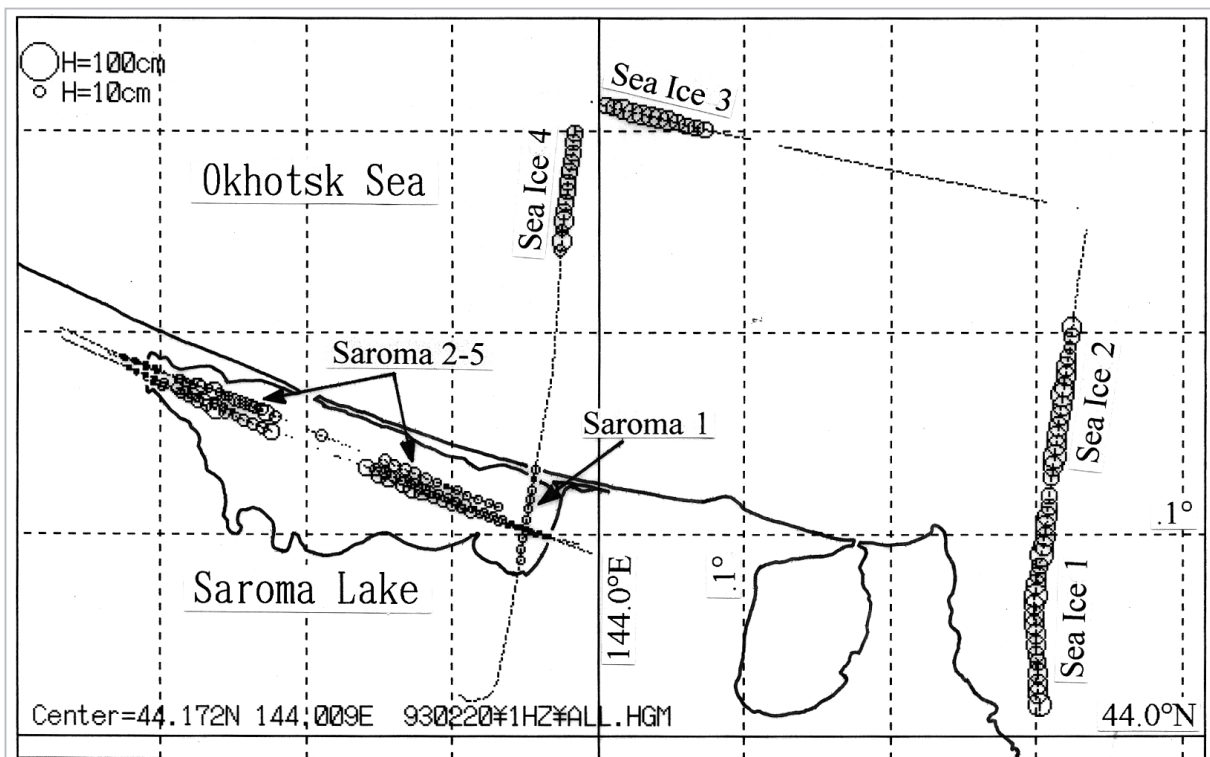The lower plotted point for each row in

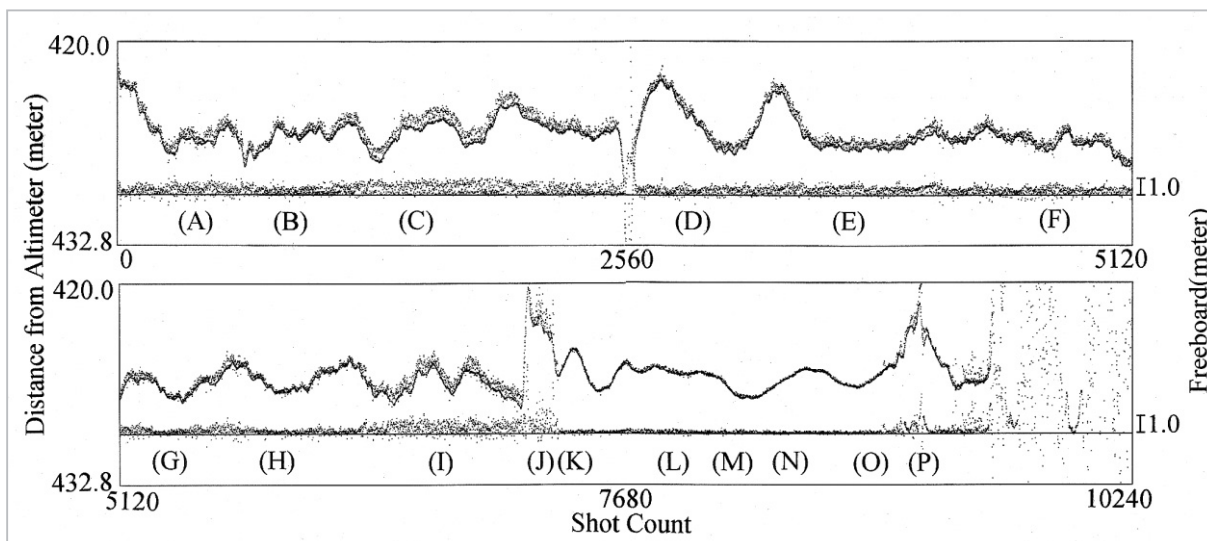**Fig.9** *Flight path for observation of drifting ice*

Fig.10 Height data and freeboard of drifting ice by flight survey

Fig.10 represents the freeboards of drifting ice measured from this estimated sea surface (right vertical axis). As shown in this graph, drifting ice data is characterized by uniform distribution within a certain freeboard width, or is distributed near the upper and lower boundaries, and a maximum freeboard of the drifting ice reaches as high as 50 cm. In significant contradiction to this data, it was reported that in a freeboard distribution of drifting ice in the Arctic Sea, the distribution of the drifting ice data decreases exponentially when the freeboard becomes higher[1 2]. It is inferred that this contradiction results from the fact that the sea ice of the Okhotsk Sea is first-year ice, since the coast of Hokkaido is located south of the boundary of freezing, whereas the sea ice in the Arctic Sea is multi-year ice, subject to repeated cycles of growth, melting, collection, and distribution. No drifting ice existed along or near the sea coast close to Saroma Lake during the day of observation; as a result, waves reached the seashore. The heights of these waves are shown in the graph; it can be seen that the height distribution is close to the normal distribution. In the sandbar, there were double cross-shaped structures to prevent erosion by the ocean current, in addition to some plant life. The altitude variation was thus large, due to vegetation. Since Saroma Lake was frozen over (except for the central portion), its surface was very smooth

and altitude variation small.

The drifting ice off the coast of Hokkaido is thin relative to arctic sea ice, and unstable due to ocean current and winds. Further, the freeboard distribution (as shown in Fig.10) differs clearly from the exponential freeboard distribution of the arctic sea ice, and the shape of the distribution varies from place to place. Therefore, it is not appropriate to study the drifting ice off the Okhotsk coast by means of freeboard distribution. We analyzed the relationship between the ice concentration and freeboard of the drifting ice. If the measured freeboard was no higher than 10 cm, it was assumed that the laser pulse had struck the sea surface; the ice concentration was thus defined every 2 seconds (every 40 pulses) as a percentage of freeboards above 10 cm. In Fig.11, the ice concentration and mean freeboard are plotted for the drifting ice, obtained by observation from 1993 to 1995. The correlation between both sets of data was excellent regardless of observation point, time, and year, and was found to distribute along a same line. Therefore, if the freeboard distribution of the drifting ice is observed with the laser altimeter, the ice concentration can be derived or estimated. Further, it is concluded that, if the specific gravities of the drifting ice above and below the sea surface are known, it becomes possible to estimate the amount of drifting ice. Details of the observations of
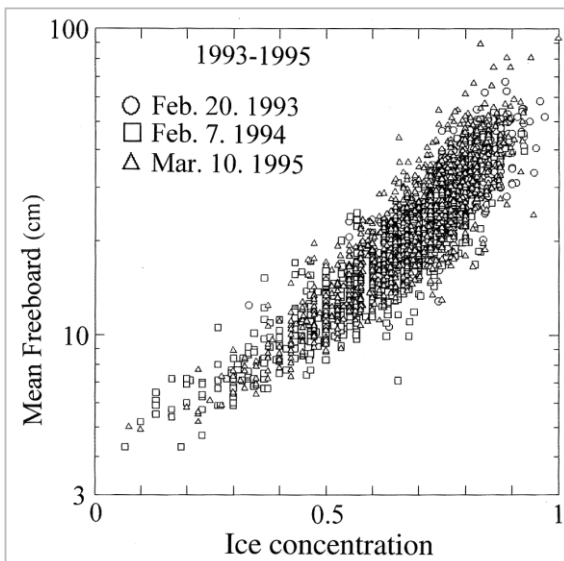
Fig.11 *Mean freeboard and concentration of drifting ice*

drifting ice and of Saroma Lake using the altimeter are included in a separate paper[1 3].

6 Basic Development of Space-Borne Laser Altimeter

As described in Chapter 3, the heterodyne laser altimeter is advantageous because it can employ low laser-transmission energy and the laser light can be transmitted in the eye-safe wavelength region. Moreover, this system possesses higher sensitivity than the direct detection system by approximately one order of magnitude. However, in heterodyne detection higher performance and stability (exceeding those required in direct detection systems) are required for the laser and receiving optical system. First, the transmitting pulsed laser and a local cw laser must both be single-frequency lasers, and their frequencies must be synchronized; second, light wave collected onto the detector through the receiving optical system must be in phase. In other words, these lasers must be of a single longitudinal mode and fundamental transverse mode and the optical collecting system must be diffraction-limited, and these characteristics must be maintained throughout the period of observation.

To realize these capabilities, we are developing a heterodyne laser altimeter system, initially for ground experiments. The most important component of this system is the lasers. Since the reflectivity of ice and snow surface decreases at wavelengths of 1 μ m and longer, it is necessary to carefully determine the wavelength. Since the flight survey has confirmed a measurement accuracy of 10 cm and eye-safety even at a wavelength of 1 μ m, the altimeter is being developed with the Nd:YAG laser. As its configuration is basically the same as the airborne altimeter, we will describe only the transmitter/receiver block and the laser which are quite different from our airborne system.
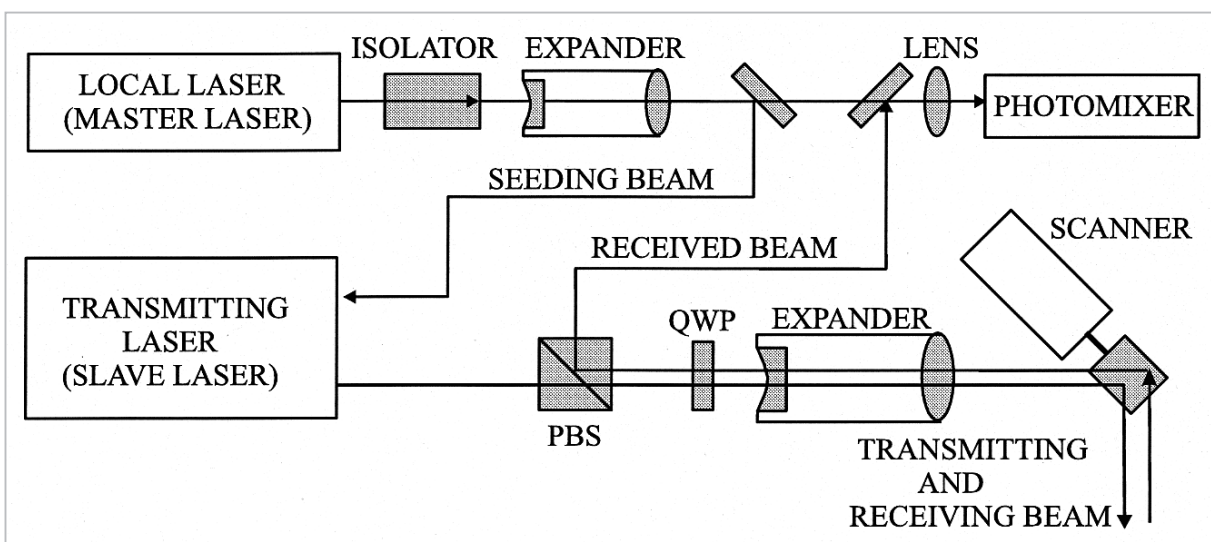

Fig.12 *Block diagram of transmitter/receiver of heterodyne laser altimeter*

6.1 Transmitter/Receiver Block

Fig.12 shows the block diagram of the transmitter/receiver of the altimeter system. The local laser is a single-frequency microchip Nd:YAG laser (CrystaLaser, IRCL-300-1064) delivering cw output of 460 mW. The output beam divergence is 4 mrad and beam diameter is 0.4 mm. This beam passes through an isolator and a beam expander, and a portion of this beam is mixed with the received light and focused onto the mixer, an InGaAs PIN photodiode (Hamamatsu Photonics K.K., G3476-01) made for the optical-communication band. The quantum efficiency at 1,064 nm is 80% and the cut-off frequency is 2 GHz. The isolator is used to cut off reflected beam from the transmitting pulsed laser, and the expander was inserted for mode matching of the local laser beam with those of the received light and the transmitting pulsed laser which is injection-locked by the local laser.

Fig.13 shows the assembled transmitter/receiver of the altimeter. The transmitting laser is under development, so only a case is shown. To adjust the receiver optics, a 240-mW portion of the local laser light was made to irradiate the surface of a rotating disk made of a white plate located 3.5 m away, and its scattered light was received to obtain the beat signal shown in Fig.14. This scattered light corresponds to scattered light from an object at a distance of 2,400 m exposed to a pulsed laser having an energy of 4 mJ and pulse width of 20 ns. Although the signal level was below the theoretical value by approximately 10 dB due to an insufficient adjustment of the local power level and the collecting optics, passable heterodyne detection was conducted. After completion of the transmitting laser, appropriate adjustments will be made.

6.2 Transmitting Pulse Laser

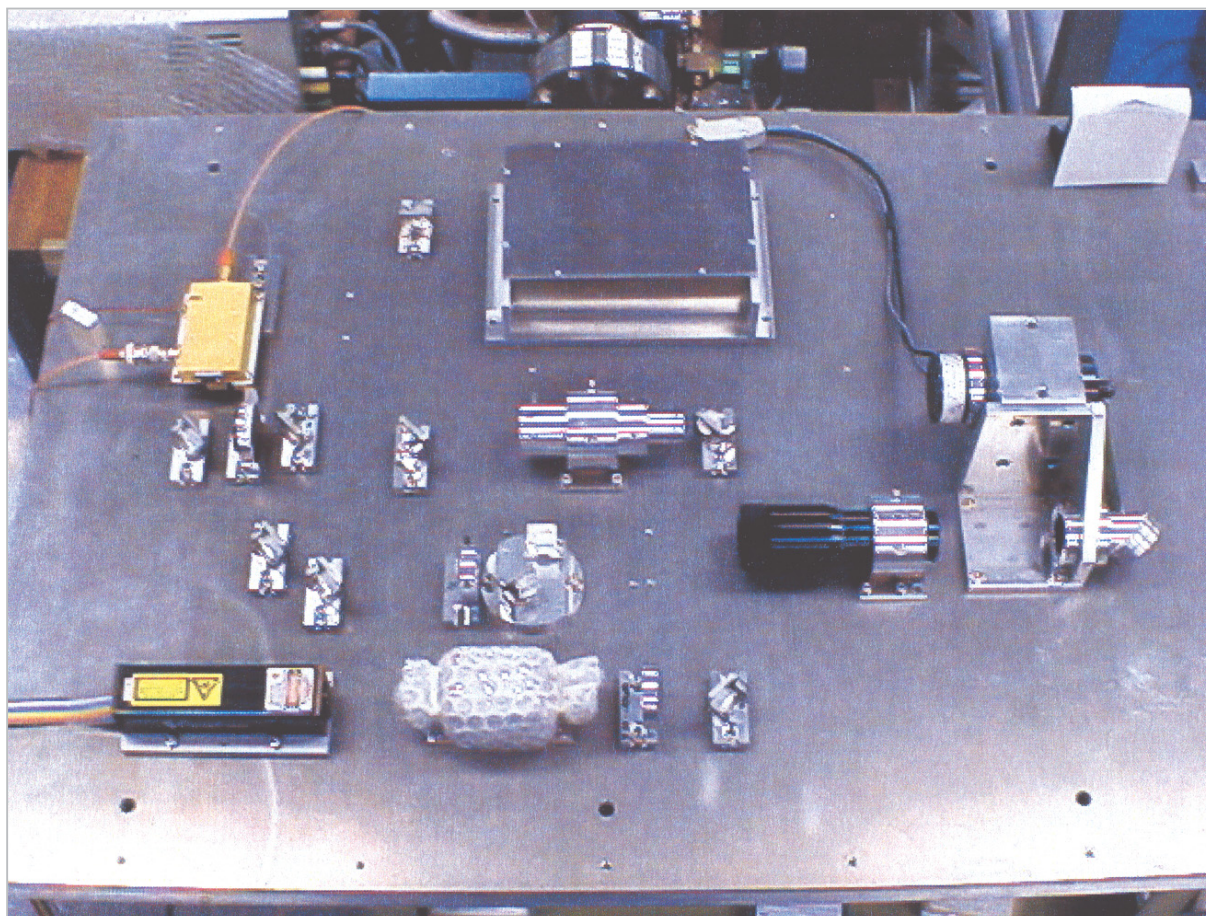For the transmitting laser, it is indispensa-

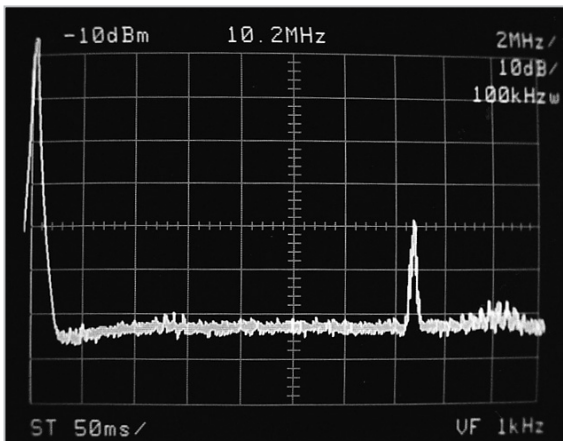**Fig.13** Transmitter/receiver of heterodyne laser altimeter

Fig.14 *Received heterodyne beat signal of transmitted cw laser beam*

ble to use a compact laser with a pulse rate of 200 pps or more that oscillates in the fundamental transverse and single longitudinal mode, and that can be injection-locked for frequency locking. This pulse rate falls between that of a flush lamp-pumped pulse laser and that of a cw-pumped pulse laser, and no appropriate commercial product is available. In addition, the configuration of the spaceborne laser differs from those of commercial products. Therefore, an appropriate transmitting laser is currently under development in our laboratory. Fig.15 shows the basic structure of this laser[14]. Two opposing Porro prisms constitute a resonator, which includes a diode-laser-pumped YAG rod, a Q-switching Pockels cell, and a polarizer. The Porro prism on the Q-switching arm is rotated by 45 degrees in azimuth angle and provides a phase shift resulting from double internal Fresnel reflections and an image reversal in the prism;

the phase shift eliminates the need for a wave plate. The degree of coupling of the output is adjusted by the rotation of azimuth angle of the prism on the laser rod arm, and the output emanates through the polarizer. Two diode lasers are arranged on the side of the rod to pump the rod.

Since the rod is pumped by the diodes only from one side, excitation distribution in the rod is extremely not uniform. However, each time the laser light travels back and forth in the resonator, the cross section of the beam rotates by twice the angle formed by the ridge lines of the two prisms; therefore, by setting a ridge line angle equal to an irrational number times 2π, any light ray passing through a certain point in the rod cross section is directed so as not to pass through that point again. After the multiple round-trips, the nonuniform excitation distribution can be averaged with respect to the laser beam around the rod's axis. With this setting, a top-hat beam with high rotational symmetry may be obtained. According to the conventional laser resonator theory, it is assumed that the laser cannot oscillate unless the light ray in the resonator returns to the initial position and angle. However, this resonator has indicated that the laser can oscillate even if the laser light ray does not return to the initial position, provided that the overall amplitude distribution agrees with the initial distribution after making a round-trip.

This resonator also displays excellent stability against mechanical distortion such as the
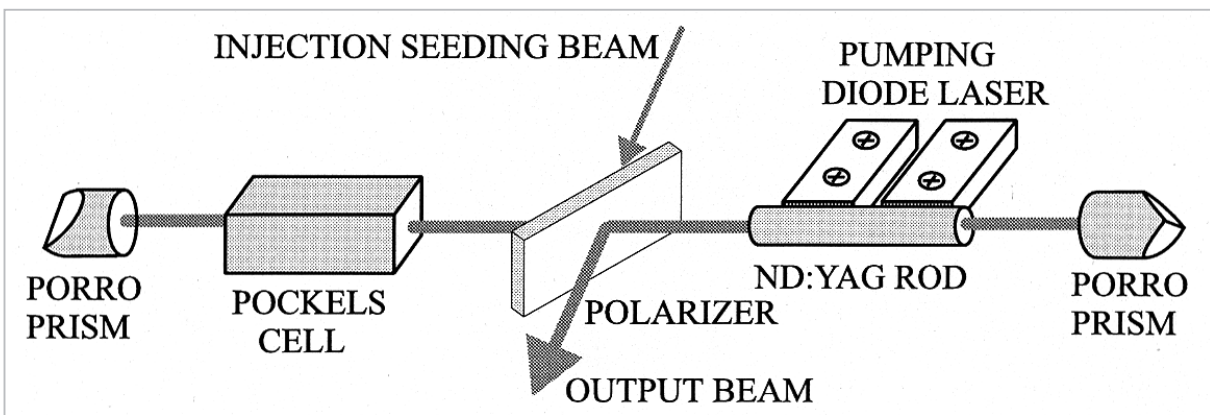

Fig.15 *Configuration of diode-pumped Q-switched Nd:YAG laser for transmitter*

same as cross-prism resonators. Furthermore, all parts are placed on the same plane, which simplifies the manufacture and assembly of the laser housing and parts holders. Heat generated in the diodes can be removed along the shortest path through the base plate. This planar construction ensures reliability in every steps of laser manufacture, adjustment, and testing.

For its satellite-borne laser, NASA has employed a zigzag-slab laser of planar construction according to the method developed for MOLA[15][16]. However, since the excitation distribution can be averaged only in the excitation direction among the two orthogonal directions in the rod cross section, the beam diameter and beam divergence of the laser differ between these two directions. The laser is thus susceptible to improvement. Furthermore, since the laser is based on a standing-wave resonator, single-frequency operation is difficult to achieve.

To achieve single-frequency operation of the laser, as required in the heterodyne detection system, the spatial hole burning of excitation distribution in the rod must be eliminated. The laser being developed eliminates the spatial hole-burning by building up the twisted mode in the rod utilizing the phase shift caused by total reflections in the Porro prism of the rod side. In this configuration, single-frequency oscillation can be achieved with a minimum number of parts. Injection locking is performed by injecting a part of the local laser light through the polarizer from the opposite direction to the laser output.

This laser used a Nd:YAG crystal of 3 to 4 diameter and 30 mm long, which was pumped by two LDs [model SDL-3231-A6 (360 W), made by SDL Corp]. The hemi-cylindrical surface of the rod on the other side of the pumping was contacted with a copper block for cooling. The heat dissipated in the rod and from the LD's is extracted to the optical bench through the base plate. The output of the laser that used the 3-mm rod was 5 mJ at a pulse frequency of 200 Hz, and a pulse width of 8 ns was obtained. Fig.16 shows a
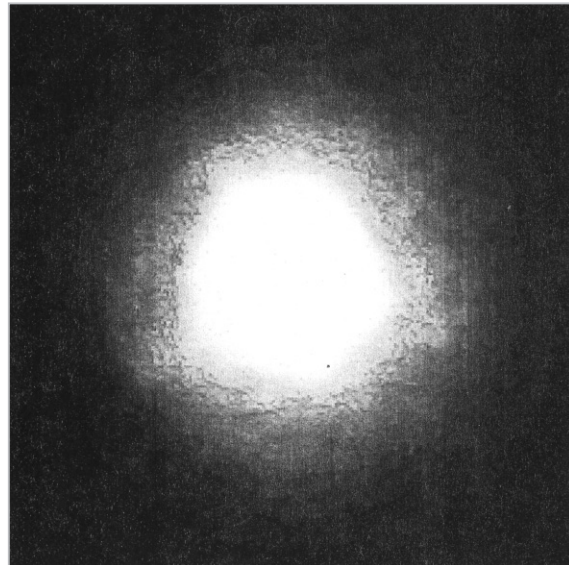

Fig.16 Beam pattern at 4 m from laser

mode pattern of the output pulses at 4 m away from the laser. Although a third-order angular mode of hexagonal symmetry appears slightly due to the intersecting plane of the Porro prism and a damage spot on the Q-switch facet, the nonuniform excitation distribution was completely averaged. Moreover, in the near-field image, a faint diffraction line caused by the ridgelines of the Porro prism is seen, along with diffraction rings from the rod circumference. From these results, it was concluded that a plane wave-front was obtained across the beam.

Fig.17 shows the relationship between the laser output energy and the pumping energy when using the 4-mm rod. The pumping duration was $200 \mu s$ and pulse repetition frequency was 100 Hz. Although the efficiency can be seen to have declined in the high-output region because LD temperature was not controlled, a differential quantum efficiency of the Q-switched oscillation of up to 24% was obtained. The predicted input/output characteristics plotted in the figure were obtained by adjusting the parameters of the laser model based on the rate equation so that the outputs agreed at an optical pump energy of 94 mJ. The model agrees well with actual laser performance. From the model, the ratio of absorbed and pump energy of the rod was estimated to be 48%. Further study to increase
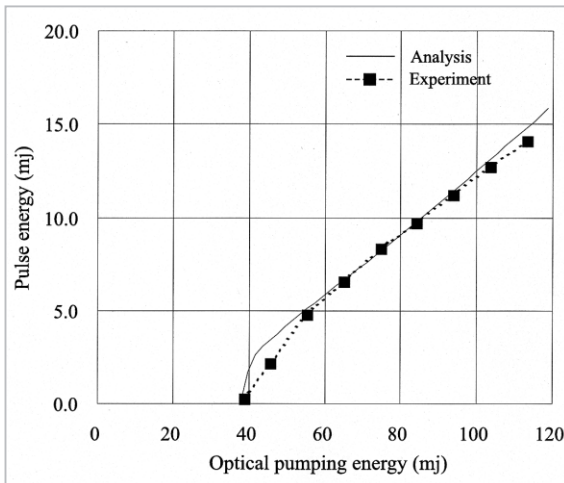
Fig.17 Pumping input and laser output

Fig.18 Waveform of Q-switched laser pulse

this efficiency is necessary.

Fig.18 shows the pulse waveform at the same pump energy of 94 mJ. The waveform is shown from the end of the pumping at which Q-switch is turned ON. The waveform and the pulse width of 28 ns which are calculated from the laser model agree well with those of the actual laser, but the calculated pulse rises up later than that of the actual pulse by 25 ns. The delay in the rise time was attributed to a discrepancy between the initial setting of number of photons in the model and the actual laser.

The output-coupling coefficient of this laser is small to compensate a relatively lower gain coefficient of the rod with 4 mm diameter. This resulted in the high Q-value of the laser resonator which stretches the laser pulse width. A small ripple in the actual waveform was caused by mode-hopping, which is a characteristic of the waveform of single-frequency pulsed lasers. Through injection-locking, this mode-hopping will disappear and the entire pulse will be forced into a single frequency. Since the laser has displayed sufficient fundamental performance as an transmitter, the altimeter is scheduled to be tested using injection-locking technique after assembly of the laser.
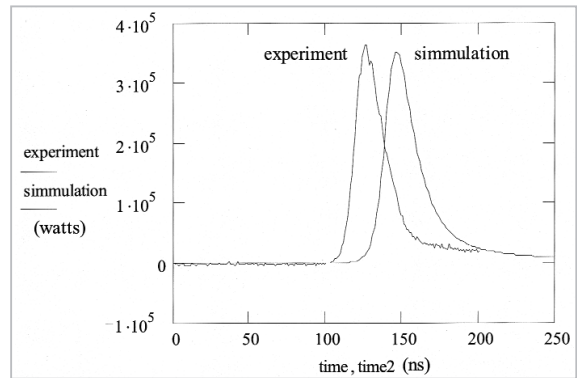
7 Conclusions

We have built and tested an airborne laser altimeter that uses a diode-pumped Nd:YAG laser for the development of a satellite-borne laser altimeter. Measurement resolution in the 5-cm range (expected from main specifications) was obtained from the results of the ground test. This altimeter was deployed on an airplane to observe ice drifting off of the Okhotsk coast of Hokkaido. It was demonstrated for the first time that a strong correlation existed between the mean freeboard and concentration of ice. For the deployment of a satellite-borne altimeter we are conducting basic study of a heterodyne laser altimeter that can provide eye safety and allow the use of a compact receiving telescope. The development results of the transmitter-receiver and transmitting laser of the heterodyne laser altimeter have presented.

8 Acknowledgment

References

1 NASA, Instrument panel report: LASA Lidar Atmospheric Sounder and Altimeter, Earth observing system reports d, p4, 1987.

2 S. C. Cohen, J. J. Degnan, J. L. Bufton, J. B. Garvin and J.B.Abshire, "The Geoscience Laser Altimetry/Ranging System", IEEE Trans. on Geosci. and Remote Sensing GE-25, pp.581-549, 1987.

3 Bufton J., "Laser Altimetry Measurements from Aircraft and Spacecraft", Proc. IEEE, 77, 463-477, 1989.

4 Abshire, J.B., X. Sun and R.S. Afzal, "Mars Orbiter Laser Altimeter: Receiver model and performance analysis", Appl. Optics, 39, 2440-2460, 2000.

5 Smith, D.E., M.T. Zuber, H.V. Frey, J.B. Garvin, J.W. Head, D.O. Muhleman, G.H. Pettengill, R.J. Phillips, S.C. Solomon, H.J. Zwally, W.B. Banerdt, T.C. Duxbury, M.P. Golombek, F.G. Lemoine, G.A. Neumann, D.D. Rowlands, O. Aharonson, P.G. Ford, A.B. Ivanov, P.J. McGovern, J.B.Abshire, R.S. Afzal, and X. Sun, "Mars Orbiter Laser Altimeter (MOLA): Experiment summary after the first year of global mapping of Mars", J. Geophys. Res., 106, 23, 689-23, 722, 2001.

6 Garvin, J., J. Bufton, J. Blair, D. Harding, S. Luthcke, J. Frawley, and D.D. Rowlands, 1998, "Observations of the Earth's topography from the Shuttle Laser Altimeter (SLA): laser-pulse echo-recovery measurement of terrestrial surfaces", Phys. Chem. Earth, 23 (9-10):1053-1068, 1998.

7 IEC825-2 and JIS C 6802.

8 Ishizu M. and T. Itabe, "Observation of sea ice in the Sea of Okhotsk by a laser altimeter", Proceedings of SPIE, 3382, pp.146-151, 1998.

9 Wolfe, W. L. and G. J. Zissis, (Eds.), in the Infrared Handbook, Figure 3-124, Environmental Research Institute of Michigan, Ann Arbor, MI, 1978.

10 McClatchy et al., Optical properties of the atmosphere, AFCRL-72-0497, AFCRL, Hanscom AFB, MA,1970.

11 O'Brien H. H., Red and near-infrared spectral reflectance of snow, Report No. 332, U.S. Army Cold Regions Research and Engineering Lab., Hanover, NH, Mar. 1975.

12 P. Wadhams, W. B. . Tucker, W. B. Krabill, R. N. Swift, J. C. Comiso and N. R. Davis, "Relation between sea ice freeboard and draft in the Arctic Basin", J. Geophys. Res., 97(C12), 20325-20334, 1992.

13 M. Ishizu, K. Mizutani and T. Itabe, "Airborne freeboard measurements of sea ice and lake ice at the sea of Okhotsk coast in 1993-95 by a laser altimeter", Int. J. of Remote Sensing, 20, pp.2461-2476, 1999.

14 Patent pending, No.400096 (2001), No.400097 (2001).

15 Afzal, R. S., "Mars observer laser altimeter: laser transmitter", Appl. Opt., 33, pp.3184-3188, 1994.

16 Errico A., C. Narrie, A. Cosentino, P. Laporta, P. Wazen and P. Maine, "Diode-pumped high-efficiency high-brightness Q-switched Nd:YAG slab laser", Opt. Lett., 22, pp.1168-1170, 1997.

ISHIZU Mitsuo

Senior Researcher, Lidar Group, Applied Research and Standards Division

Laser Remote Sensing